Journal of

Applied and Computational Mechanics

Shahid Chamran
University of Ahvaz

Research Paper

Towards an Optimization of the Spectral Collocation Method with a New Balancing Algorithm for Plotting Dispersion Curves of Composites with Large Numbers of Layers

Moussa Mekkaoui[1], Salah Nissabouri[2], Hassan Rhimini[1]

[1] Laboratory of Mechanics, Engineering and Innovation, National High School of Electricity and Mechanics, Hassan II University, Casablanca, Morocco
Email: moussa.mekkaoui@ensem.ac.ma (M.M.); h.rhimini@ensem.ac.ma (H.R.)

[2] M2S2I Laboratory, Department of Mechanical engineering, ENSET-Mohammedia, Hassan II University, Mohammedia, Morocco
Email: SALAH.NISSABOURI@univh2c.ma (S.N.)

Abstract. This article proposes a new algorithm for computing dispersion curves of ultrasonic guided waves in multi-layered composites with large number of layers. The algorithm is based on balancing the eigenvalue problem of the Spectral Collocation Method (SCM) formulation. The SCM has proven effective in analyzing single-layer and simple waveguides. However, it struggles with large multi-layer structures due to numerical instability caused by irregular and sparse matrices in the eigenvalue problem. The proposed algorithm for balancing has significantly reduced both the conditioning measure and the matrix norm in the matrix system. The optimization of spectral formulation enables accurate calculation of dispersion curves and characterization of displacement/stress profiles using Matlab software. This precise characterization and mode separation are essential for selecting ultrasonic sensors for damage detection. A comparison was made with Dispersion Calculator (DC) software. The algorithm was first validated using a hybrid multi-layered composite [CFRP-Al-CFRP-Al], which was successful. The validated algorithm was then quantitatively evaluated using a cross-play laminate T800M913 [0/90/0/90] in terms of three parameters: Number of collocation points, wave propagation direction and thickness. The algorithm is then applied to a large number of layers using three configurations: Symmetric layup T80M913[0/90]$_{10s}$, hybrid layup [CFRP-Al]$_{50}$ and challenging layup T800M913[0/90]$_{100}$. The study found that the balancing algorithm, when combined with the SCM, is effective for structures with a large number of layers. Finally, optimizing the SCM will enhance its competitiveness as an effective tool in ultrasonic non-destructive testing for the studied structures of great industrial interest.

Keywords: Dispersion curves, Spectral collocation method, Balancing eigenvalue problem. Guided waves, Multi-layered composites.

1. Introduction

In the field of Non-Destructive Testing (NDT) [1], the study of Ultrasonic Guided Waves (UGW) in solid media has gained significant importance. Researchers have made tremendous progress in using mode and frequency selection to address various challenges in applications for pipe, rail, and plate inspection, as well as numerous multilayer engineering structures. In order to achieve long-distance inspection and monitoring of layered structures, it is necessary to study the propagation characteristics of guided waves in these structures. In this context, Lamb [2] waves are widely used in NDT. They are dispersive and have the unique property of moving the entire thickness of the medium. Therefore, the accurate calculation of dispersion curves and the associated displacement and stress profiles is necessary for the study of Lamb wave propagation to ensure reliable materials testing.

Historically, Thomson [3] was the first to introduce the method in 1950 to solve the problem of wave propagation in a layered medium composed of an arbitrary number of isotropic layers. This technique, adopted and corrected by Haskell [4] in 1953, is based on the Transfer Matrix Method (TMM) formulation. Nayfeh [5] in 1991 and Knopoff [6] in 1964 developed the Global Matrix Method (GMM) formulation. The presence of singular matrices for which the inverse is undefined causes the numerical instability of the TMM formulation. Rokhlin and Wang [7] in 2001 rearranged the transfer matrix formulation and introduced the Stiffness Matrix Method (SMM). A pertinent reference that examines various aspects of the multilayer problem in flat geometry in [8-10]. These approaches, based on numerical solution, present shortcomings such as, apparent crossing between adjacent branches especially at high frequency limits, missing modes, instability due to the well-known problem of large frequency thickness parameter as mentioned in [5, 7] and the high computational cost in the case of complex and multi-layered structures. As a numerical method, Finite Element Method (FEM) has been proposed to extract dispersion curves in a variety of structures [11-13]. For example, Manconi

[14] used FEM to determine the dispersion curves of a laminated sandwich. The Semi-Analytical Finite-Element Method (SAFE) [15-17] has been proposed as an alternative method that requires only a two-dimensional discretization of the cross section, as opposed to the three-dimensional discretization of the entire waveguide required by FEM. Another numerical method used to obtain the dispersion curves is called the Legendre Orthogonal Polynomial Method [18]. This approach expresses the shape of the solution by using an orthonormal basis for the expansion of the displacement field values.

A new and promising approach to mode dispersion modeling is introduced, the Spectral Collocation Method (SCM). The SCM is an efficient tool for solving partial differential equations. The SCM reduces the problem to a compact matrix eigenvalue problem by accurately approximating the derivative operators of the equation of motion with differentiation matrices. Several papers have been published illustrating the use of the spectral method to determine the UGW dispersion curves. For example, Adamou [19] was among the first to evaluate the robustness of the method by dealing with anisotropic, inhomogeneous, and multilayer media. Karpfinger [20, 21] described an algorithm for calculating propagating modes in cylindrical structures. Quintanilla [22] studied the symmetry and coupling properties of solutions in general anisotropic multilayer waveguides. A recent work using the SCM to study sandwiched waveguides is in [23]. The SCM approach studied here guarantees that none of the modes are missed, and eigenvectors representing accurate approximations of the mode shapes are automatically generated with the eigenvalues.

When studying multilayer plates, the use of the SCM becomes more efficient due to the persistent problems in matrix analytical methods. However, applying the method in this context is still a challenging task. The addition of boundary conditions and interfaces to the matrix system of the eigenvalue problem $Lx = \lambda Mx$ can cause ill-conditioning, even when an inverse matrix exists. Some matrices are practically singular during the calculation of the problem's eigenvalues with spectral formulation, making the calculation vulnerable to numerical errors. Furthermore, as the size of the matrices increases with a higher number of layers, the matrix system becomes very large and sparse. Consequently, the solutions found are inaccurate, with spurious eigenvalues. Numerical instabilities have been observed in the SCM algorithms proposed by [20, 22]. In this study, we addressed the issue of numerical instabilities by balancing the L and M matrices before calculating the SCM eigenvalues. As a result, the process of obtaining dispersion curves for multilayer composites is now reliable, precise, and covers a wide variety of structures. These findings are presented in this work.

The balancing technique is based on bilateral diagonal transformations and permutations on the L and M matrix system. The matrices consequently become well-conditioned and non-regular. The remainder of the paper provides a clear explanation of the proposed algorithm based on Ward's program [24]. Consequently, the new balanced SCM becomes stable for n layers and improves the accuracy and robustness of the dispersion curve calculation.

The paper is structured as follows: Section II describes the numerical SCM used to resolve characteristic equations of waveguides in multi-layered composites. We then focus on the balancing algorithm of the general eigenvalue problem, which we combine with the plotting program of SCM for the first time. In Section III, we provide a brief overview of the DC software [25] used to validate the plotted dispersion curves. In Section IV, we first assess the efficiency of the balancing algorithm by calculating matrix conditioning functions and relative errors. We then evaluate the impact of the number of collocation points (N), wave propagation direction, and thickness on curve precision and running time. To validate our findings, we compute dispersion curves for various cases of multi-layered composites. At a specific couple frequency-wave number (f,k), we calculate the displacements and stress profiles of the first fundamental modes. In addition, we investigate the case of a large number of layers, up to 200, which challenges several methods and software programs in this field. Finally, we discuss the results by comparing them with DC's curves.

2. Spectral Collocation Method and Balancing Algorithm

2.1. SCM formulation for multi-layered composites

We start by explaining the method used in our study. The spectral collocation point method is an efficient and accurate tool for solving partial differential equations. It utilizes differentiation matrices that provide a spectral precision approximation of the derivative operators. These differentiation matrices can be computed using interpolants, such as Chebyshev, Fourier, Hermitian, or others, that can be precisely differentiated. Subsequently, this section demonstrates how to calculate the dispersion of waves propagating in multilayer structures presented in Fig. 1(a), made of Carbon Fiber Reinforced Polymer (CFRP), using Chebyshev collocation points and differentiation matrices.
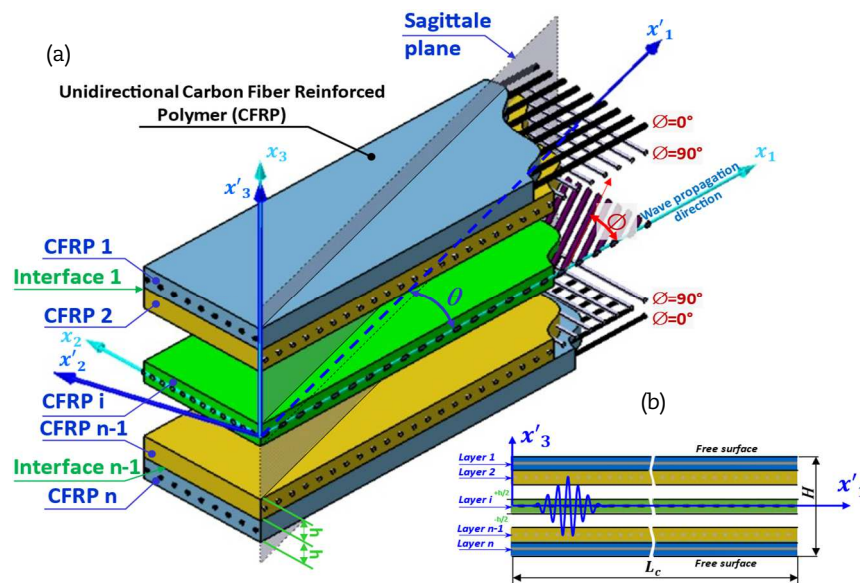

Fig. 1. Schematic of a multi-layered composite made of CFRP: (a) 3D representation, with x_i' the coordinate system for wave propagation and the global coordinate system x_i, i=1, 2, 3. The layers have a constant thickness of h, (b) 2D representation of n-layers system and the total thickness of H and length of L_c.

We consider the ith layer in Fig. 1(b) as a homogeneous anisotropic plate of thickness h with the axis x_1 as the direction of wave propagation.

The equation of motion for a homogeneous anisotropic medium with linear elastic behavior is given by:

$$\frac{\partial \sigma_{ij}}{\partial x_i} = \rho \frac{\partial^2 u_i}{\partial t^2}, \tag{1}$$

The relationship between the stress tensor field and the strain tensor field is written as:

$$\sigma_{ij} = C_{ijkl}\, \varepsilon_{kl}, \tag{2}$$

where C_{ijkl} is the stiffness tensor of the plate and the strain tensor field, ε_{ij}, is written as function of the displacement vector field, u_j, as:

$$\varepsilon_{kl} = \frac{1}{2}\left(\frac{\partial u_k}{\partial x_l} + \frac{\partial u_l}{\partial x_k}\right), \tag{3}$$

And the components of displacement field can be written as:

$$u_j = U_j\left(x_3\right) e^{i(kx_1 - \omega t)}; \qquad j = 1,2,3 \tag{4}$$

with ω is the angular frequency. The Chebyshev interpolation method, as described by Weideman and Reddy [26], was used for spectral resolution. The collocation points' coordinates are defined non-uniformly in the interval [-1, 1] as:

$$x_3^{(i)} = \cos\left(\frac{(i-1)\pi}{N-1}\right); \qquad i = 1,...,N \tag{5}$$

Figure 2 illustrates the discretization in a layer thickness of the nth layer belonging to a multilayer used subsequently, and the components of the displacement field are also discretized into N points along the local axis x_3:

$$\left(U_1, U_2, U_3\right) = \left(\{U_{11}, U_{12},...,U_{1N}\}^T, \{U_{21}, U_{22},...,U_{2N}\}^T, \{U_{31}, U_{32},...,U_{3N}\}^T\right), \tag{6}$$

And the differential operators defined in x_3 are approximated by Chebyshev differentiation matrices (DM) generated in the domain [-h/2, h/2]. The order of derivation is noted n:

$$\frac{\partial^n}{\partial x_3^{\,n}} \;\rightarrow\; D^n = [DM]_{N\times N}^{\,n}, \tag{7}$$

A detailed description of the SCM can be found in [27–29]. Consequentially, we end up with a system of three equations of motion and six equations for the boundary conditions.

The propagation Eq. (1) can be written in the following matrix form, where the unknowns are the vectors U_j:

$$\begin{bmatrix} L_{11} & L_{12} & L_{13} \\ L_{21} & L_{22} & L_{23} \\ L_{31} & L_{32} & L_{33} \end{bmatrix}_{3N\times 3N} \begin{Bmatrix} U_1 \\ U_2 \\ U_3 \end{Bmatrix}_{3N\times 1} = \omega^2 \begin{bmatrix} -\rho I & 0 & 0 \\ 0 & -\rho I & 0 \\ 0 & 0 & -\rho I \end{bmatrix} \begin{Bmatrix} U_1 \\ U_2 \\ U_3 \end{Bmatrix}, \tag{8}$$

Or, more concisely,

$$L\left(k\right) U = \omega^2 M U, \tag{9}$$

The expressions of the elements of matrix L are:

$$\begin{aligned}
L_{12} &= C_{45}D^{(2)} - C_{16}k^2 I + (C_{14} + C_{56})kiD^{(1)}, \\
L_{13} &= C_{35}D^{(2)} - C_{15}k^2 I + (C_{13} + C_{55})kiD^{(1)}, \\
L_{23} &= C_{34}D^{(2)} - C_{56}k^2 I + (C_{36} + C_{45})kiD^{(1)}, \\
L_{11} &= C_{55}D^{(2)} - C_{11}k^2 I + 2C_{15}kiD^{(1)}, \\
L_{22} &= C_{44}D^{(2)} - C_{66}k^2 I + 2C_{46}kiD^{(1)}, \\
L_{33} &= C_{33}D^{(2)} - C_{55}k^2 I + 2C_{35}kiD^{(1)}, \\
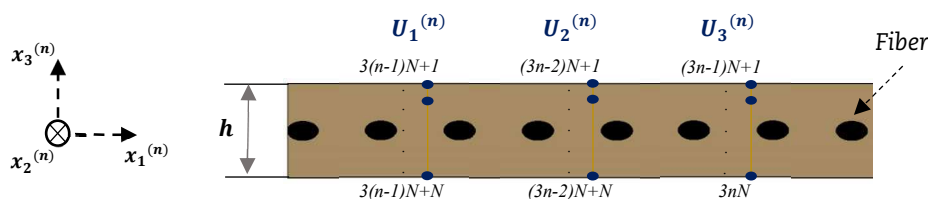L_{21} &= L_{12}; L_{31} = L_{13}; L_{32} = L_{23},
\end{aligned} \tag{10}$$

Fig. 2. The nth infinite single layer with N collocation points discretization for each displacement component $U_i^{(n)}$ and its local coordinate system $x_i^{(n)}$. With the thickness of h.

With *I* the identity matrix and C_{KL} the elastic stiffness constants. The $N \times N$ (DM) matrices $D^{(1)}$ and $D^{(2)}$ are generated using the Matlab function chebdif [30].

Then, we proceed to a discretization of Eqs. (2) and (3) and a rearrangement of their terms, so the expressions of the stress matrix can be represented in matrix notation:

$$(\sigma_{33}, \sigma_{13}, \sigma_{23})^T = [S(k)]\{U\} = \begin{bmatrix} S_1 & S_2 & S_3 \\ S_4 & S_5 & S_6 \\ S_7 & S_8 & S_9 \end{bmatrix} \begin{Bmatrix} U_1 \\ U_2 \\ U_3 \end{Bmatrix}_{N \times 1} \tag{11}$$

The expressions of the S matrix elements are:

$$\begin{aligned}
S_1 &= C_{13}kiI + C_{35}D^{(1)}, \\
S_2 &= C_{36}kiI + C_{34}D^{(1)}, \\
S_3 &= C_{35}kiI + C_{33}D^{(1)}, \\
S_4 &= C_{14}kiI + C_{45}D^{(1)}, \\
S_5 &= C_{46}kiI + C_{44}D^{(1)}, \\
S_6 &= C_{45}kiI + C_{34}D^{(1)}, \\
S_7 &= C_{15}kiI + C_{55}D^{(1)}, \\
S_8 &= C_{56}kiI + C_{45}D^{(1)}, \\
S_9 &= C_{55}kiI + C_{35}D^{(1)},
\end{aligned} \tag{12}$$

The eigenvalue problem in Eq. (9) is resolved by implementing the boundary conditions on the free surfaces of the plate. In the remainder of this paper, we explain the method for solving this type of problem in a multilayer structure system.

The formulation for a multi-layered composite in SCM adopts the assembly technique of many systems from the same detailed model in Eq. (8). For a multilayer composite consisting of *n* layers, Fig. 1 shows an example of a stack of layers with fiber orientations of 0 and 90 degrees. The equation analogous to Eq. (8) is presented below:

$$\begin{bmatrix} L^{(1)} & 0 & \cdots & 0 \\ 0 & L^{(2)} & \cdots & 0 \\ \vdots & \vdots & \ddots & \vdots \\ 0 & 0 & \cdots & L^{(n)} \end{bmatrix}_{3nN \times 3nN} \begin{Bmatrix} U^{(1)} \\ U^{(2)} \\ \vdots \\ U^{(n)} \end{Bmatrix}_{3nN \times 1} = \omega^2 \begin{bmatrix} M^{(1)} & 0 & \cdots & 0 \\ 0 & M^{(2)} & \cdots & 0 \\ \vdots & \vdots & \ddots & \vdots \\ 0 & 0 & \cdots & M^{(n)} \end{bmatrix}_{3nN \times 3nN} \begin{Bmatrix} U^{(1)} \\ U^{(2)} \\ \vdots \\ U^{(n)} \end{Bmatrix}_{3nN \times 1} \tag{13}$$

Each of the labeled matrices $L^{(i)}$, $M^{(i)}$ and $U^{(i)}$ (where $i = 1...n$, indicates the block matrices and the displacement vectors in each layer *i*) has the monolayer form shown in Eq. (8). Or, more concisely:

$$[\mathcal{L}(k)]\{\widehat{U}\} = \omega^2[\mathcal{M}]\{\widehat{U}\}, \tag{14}$$

Before proceeding with assembly, each individual layer undergoes the following transformation: the material properties of the nth layer expressed in the local coordinate $x_i^{(n)}$ ($i = 1, 2, 3$), must be transformed in the coordinate system x_i ($i = 1, 2, 3$) using a tensor rotation. The density of the material is a scalar and remains invariant before and after the rotation. The elastic constant is a fourth-order tensor, and the rotation formula is expressed as follows:

$$C'_{mnop} = \mathcal{R}_{mi}\mathcal{R}_{nj}\mathcal{R}_{ok}\mathcal{R}_{pl}C_{ijkl}, \tag{15}$$

Here $\mathcal{R}$ is the transformation matrix as:

$$\mathcal{R}_{mi} = \begin{bmatrix} \cos(\theta_j) & \sin(\theta_j) & 0 \\ -\sin(\theta_j) & \cos(\theta_j) & 0 \\ 0 & 0 & 1 \end{bmatrix}, \tag{16}$$
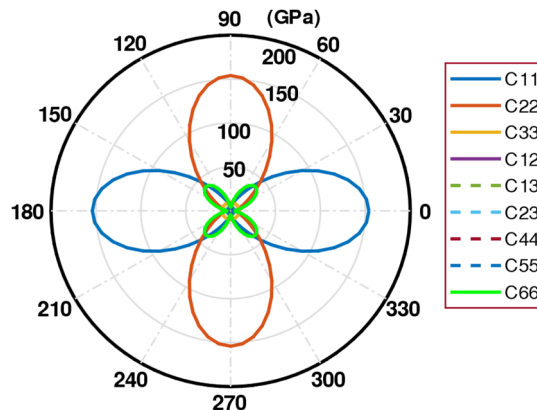

Fig. 3. Transformation stiffness tensor components versus *θ* of transversely isotropic plate.

and the angle between x_1 and $x_1^{(n)}$ (fiber direction of the nth layer) is $\varnothing_i$, C_{ijkl} and C'_{mnop} are the stiffness tensor before and after transformation, respectively.

To illustrate the transformation required on each layer's stiffness matrix before calculation, consider the example of configuration T800M913[0/90/0/90] and a propagation direction with angle $\theta = 45$ degrees. In this case, apply rotation angles $\theta_i = 45, -45, 45, -45$ to achieve an effective configuration of [45/-45/45/-45]. Table 5 lists the elastic constants of the transversely isotropic plate, and Fig. 3 illustrates their variation with respect to the angle θ.

As shown in Fig. 1, the faces of the multilayer are located at $x'_3 = H/2$ and $x'_3 = -H/2$ (H is the multilayer total thickness) and are free in stress. Therefore, the boundary conditions (BC) are expressed as:

$$\sigma_{33}^{(1)}(H/2) = \sigma_{31}^{(1)}(H/2) = \sigma_{32}^{(1)}(H/2) = 0, \qquad \text{(the top of the first layer)}$$
$$\sigma_{33}^{(n)}(-H/2) = \sigma_{31}^{(n)}(-H/2) = \sigma_{32}^{(n)}(-H/2) = 0, \qquad \text{(the button of the nth layer)}$$

$$(17)$$

We also impose continuity conditions across interfaces. For an interface, let's say the first interface between layers 1 and 2, the continuity conditions of the stress tensor field and the continuity conditions at a perfect interface for displacement fields are:

$$\left. \sigma_{33}^{(1)} - \sigma_{33}^{(2)} \right|_{x_3=1st} = 0 \qquad\qquad \left. u_1^{(1)} - u_1^{(2)} \right|_{x_3=1st} = 0,$$
$$\left. \sigma_{31}^{(1)} - \sigma_{31}^{(2)} \right|_{x_3=1st} = 0 \qquad ; \qquad \left. u_2^{(1)} - u_2^{(2)} \right|_{x_3=1st} = 0, \qquad (18)$$
$$\left. \sigma_{32}^{(1)} - \sigma_{32}^{(2)} \right|_{x_3=1st} = 0 \qquad\qquad \left. u_3^{(1)} - u_3^{(2)} \right|_{x_3=1st} = 0,$$

where $x_3 = 1st$ means evaluation at the first interface.

This gives a total of six equations for each interface. So, for a system of n layers, we have n-1 interfaces and $6n$-6 interface equations, plus six boundary conditions, for a total of $6n$ equations, which must replace the appropriate lines in the matrix system Eq. (13). The following Fig. 4 illustrates how to implement the boundary conditions BC at the upper and bottom layers, the stress continuity interface conditions IC (SC.i-j), and the displacement continuity interface conditions IC (DC.i-j) between two adjacent layers i and j. The modified line numbers are indicated in the same figure and respect the non-overlapping condition. The method was programmed in Matlab, and the resulting matrices require a balancing phase, which will be detailed later in the paper.
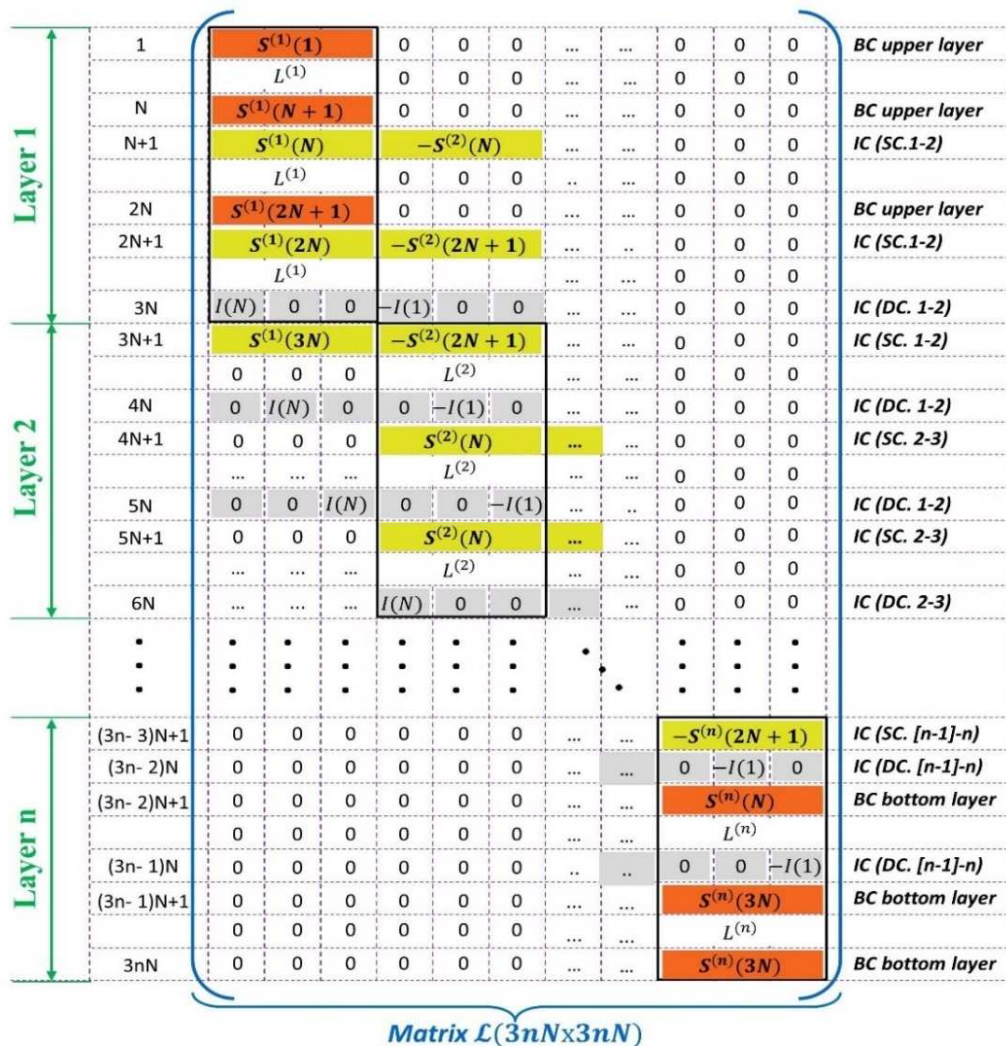

Fig. 4. Construction of the global matrix $\mathcal{L}$ following the collocation scheme for a n-layers matrix system. The external boundary conditions (BC) as well as the interface conditions (IC) are introduced in lines indicated by the left column. The empty boxes represent zeros in the global matrix $\mathcal{L}$.

with:

I(i) corresponds to the ith row of the I identity matrix of dimension NxN.

$S^{(j)}(i)$ corresponds to the ith line of the S matrix of the jth layer.

Similarly, the same lines where the boundary and interface conditions are introduced into the matrix $\mathcal{L}$, are replaced in the matrix $\mathcal{M}$ by lines filled with zeros.

2.2. Balancing the general eigenvalue problem

After introducing interface conditions in a multilayer case, non-symmetric and sparse matrices arise, leading to several incorrect and infinite eigenvalues and unstable results. To achieve the expected precision of QZ-type algorithms for solving this type of generalized eigenvalue problem, we balanced matrices $\mathcal{L}$ and $\mathcal{M}$ using a balancing algorithm before solving the matrix system in Eq. (14). The method of balancing is based on diagonal bidirectional permutations and transformations that reduce the norm of a matrix or the condition numbers of a subset of L-eigenvalues. According to Ward [24], the algorithm for the three-step balancing program is shown in the above graphic. The accuracy of the calculated frequencies has significantly improved, enabling precise plots of the dispersion curves as shown in the results section.

We begin by addressing an initial eigenvalue problem that needs to be balanced in three steps:

1. $\mathcal{L}_{11}, \mathcal{L}_{33}, \mathcal{M}_{11},$ and $\mathcal{M}_{33}$ are upper triangular matrices allowing to find certain eigenvalues, the others are the eigenvalues ω of the reduced problem $A_{22}x = \omega^2 B_{22}x$. Otherwise, $\mathcal{L}_{22} = \mathcal{L}$, and $\mathcal{M}_{22} = \mathcal{M}$ and the other submatrices do not exist. If $\mathcal{L}$ and $\mathcal{M}$ can transform into higher triangular form, then $\mathcal{L}_{22}$ and $\mathcal{M}_{22}$ do not exist and all eigenvalues ω have been found.

2. H_1 and H_2 are diagonal matrices. A generalized conjugate gradient technique is used for scaling.

3. In order for the ratio of the column norms of $\mathcal{L}J_2$ to the corresponding column norms of $\mathcal{M}J_2$ to appear in non-increasing order, the grading method first determines the permutation matrix J_2. Then J_1 is established in a way that the line norm ratio of $J_1\mathcal{L}J_2$ to $J_1\mathcal{M}J_2$ appears in a non-increasing order.

In the final step, the original problem of $\mathcal{L}U = \omega^2 \mathcal{M}U$ is transformed into the problem of $\mathcal{L}'V = \omega^2 \mathcal{M}'V$. If only the eigenvalues are desired, the issue can be simplified by just taking into account the matrices $J_1H_1\mathcal{L}_{22}H_2J_2$ and $J_1H_1\mathcal{M}_{22}H_2J_2$. The matrices are calculated in the established Matlab program:

$$T_1 = J_1H_1Q_1 \qquad \text{and} \qquad T_2 = Q_2H_2J_2 , \qquad\qquad (19)$$
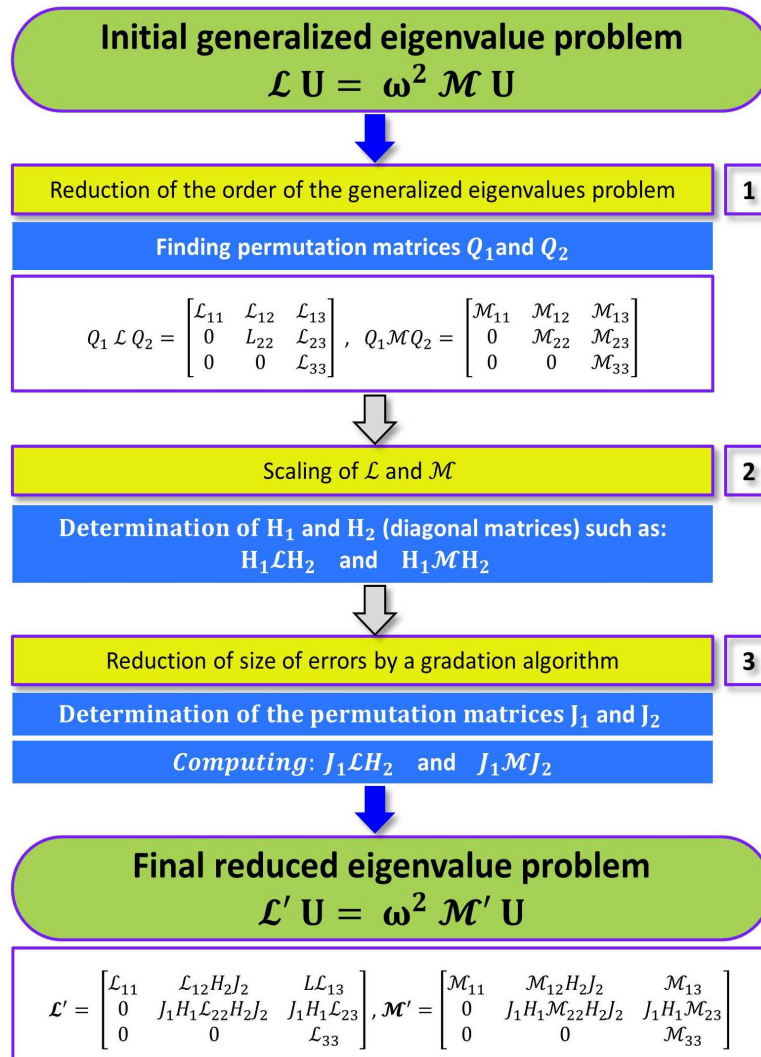

Fig. 5. The flow chart algorithm of Balancing the eigenvalue problem resulting from the multilayered composite SCM formulation.

And, the equations balance the matrices $\mathcal{L}$ and $\mathcal{M}$:

$$T_1 \mathcal{L} T_2 \qquad \text{and} \qquad T_1 \mathcal{M} T_2 , \tag{20}$$

We use an inverse transformation to base our calculations on the eigenvectors V to determine the eigenvectors U:

$$U = T_2 \begin{Bmatrix} V_1 \\ V_2 \\ V_3 \end{Bmatrix}, \tag{21}$$

After the balancing phase, a stable eigenvalue problem is obtained in terms of frequency ω:

$$\mathcal{L}' V = \omega^2 \, \mathcal{M}' V, \tag{22}$$

2.3. Proposed computational algorithm for multi-layered composites

Equation (22) allows for the calculation of propagating modes (Lamb and SH) in a material with multiple layers. The proposed algorithm, which combines the SCM and balancing technique, is implemented using Matlab software and summarized in Fig. 6.
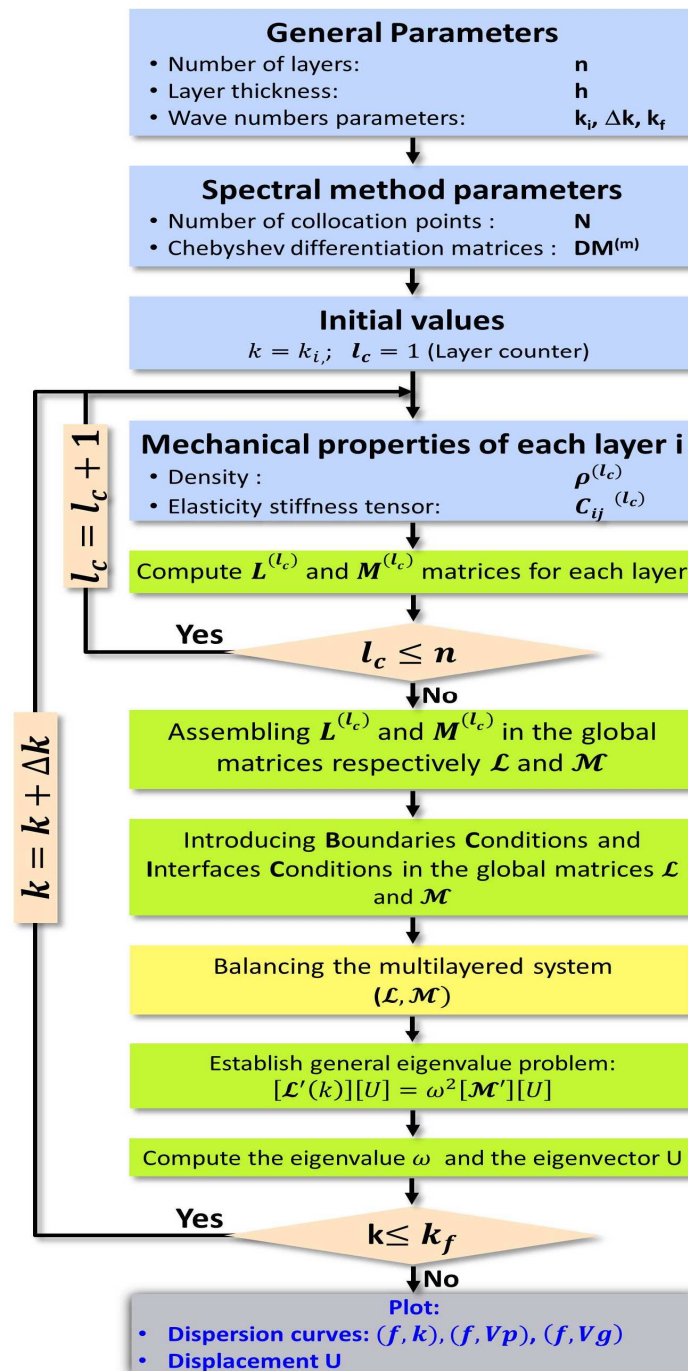

Fig. 6. The flow chart algorithm of plotting dispersion curves by SCM for layered composite.

Table 1. Proprieties of the unidirectional CFRP layer.

C_{11}	C_{22}	C_{33}	C_{12}	C_{13}	C_{23}	C_{44}	C_{55}	C_{66}	e	ρ
143.8	13.3	13.3	6.2	6.2	6.2	3.6	5.7	5.7	1	1.56

Table 2. Matrix L norm variation with balancing.

	Before balancing		*After balancing*	
N	*Norm*	*Cond*	*Norm*	*Cond*
10	1.7211e+20	1.3755e+21	810.7410	1.3536e+5
20	3.2416e+21	5.1252e+21	2.9413e+3	1.1307e+6

Table 3. Relative errors of the eigenvalues generated by the spectral method for the mth first modes ($m = 10$), ω_1 without using the balanced matrices and ω_2 with using the balanced matrices, compared to the DC's values ω_{DC}, in the CFRP-Al multilayer with wavenumber $k = 1\ rad/mm$. The spectral method used $N = 20$.

m	ω_1 (kHz)	ω_2 (kHz)	ω_{DC} (kHz)	RE (without balancing)	RE (with balancing)
1	0.00	328.88	329	100	0.03
2	322.53	406.21	406	20.56	0.05
3	384.50	478.21	478	19.56	0.04
4	384.50	487.45	486	20.88	0.29
5	412.59	592.00	590	30.07	0.33
6	526.41	811.47	811	35.09	0.06
7	580.52	844.82	840	30.89	0.06
8	0.00	930.56	930	100	0.06
9	0.00	1031.10	1031	100	0.01
10	800.93	1143.08	1137	29.56	0.53

The initial two steps require setting the model's general and spectral parameters. Following that, the $\mathcal{L}$ and $\mathcal{M}$ matrices are constructed for each layer in a loop with a step dependent on the wave number k. Finally, the global matrices are assembled and adjusted by introducing boundary and interface conditions. This balancing algorithm establishes the general eigenvalue problem, and the matrix system is transformed into a non-regular and well-conditioned state, allowing for resolution. The standard MATLAB eigenvalue function is used to calculate the eigenvalues ω and eigenvectors U for each value of k. Finally, dispersion curves and displacement profiles are plotted for a selected wave number interval.

For all types of composites, the balancing stage ensures the stability and reliability of the SCM formulation.

3. Dispersion Calculator Software

The Dispersion Calculator (DC) [25] is a validated stand-alone program that computes guided wave dispersion and mode shapes in plates and multi-layered anisotropic laminates. The outstanding book of Nayfeh [31] including the TMM served as the framework for the programming of the DC. It uses the Rayleigh-Lamb equations and the SMM. Another well-known software in this field is DISPERSE, which is based on the GMM and was developed by Lowe [8] and Pavlakovic [32]. It has a computational limitation of approximately 60 maximum layers. Therefore, DC, which has over 400 layers, is an excellent option for comparing our plots and evaluating the accuracy and robustness of our SCM formulation with the new balancing algorithm.

As already mentioned, the DC software is based on the matrix analytical approach of the SMM, which relates the stress components at the bottom and top of the layer to the displacement at the bottom and top of the layer. An advanced recursive algorithm is used to obtain the stiffness matrix for the whole composite. For further details, refer to [5, 28].

4. Results and Discussion

The algorithm presented in Fig. 6 is utilized to calculate the desired solutions for all types of composite structures. The study investigates four distinct cases:

- Hybrid multi-layered composite [CFRP-Al]$_x$
- Asymmetric transversely isotropic multi-layered composite T800M913 [0/90]$_x$
- Symmetric transversely isotropic multi-layered composite T800M913 [0/90]$_{10s}$
- Multi-layered composite with high number of layers T800M913 [0/90]$_{100}$

To validate the algorithm, the first material is used before plotting dispersion curves. Then, a parametric study is conducted using the remaining materials to compare the effectiveness and stability of our proposed algorithm with DC software. For the multi-layered composites, the transversely isotropic material was rotated using Eq. (16) based on the specific layup for each case. The layups used here have a repeating sequence indicated by the subscript number x.

4.1. Hybrid multi-layer composites [CFRP-Al]$_x$

4.1.1. Hybrid multi-layer composites [CFRP-Al- CFRP-Al]

For model validation, a complex hybrid multi-layered composite of four layers is used. The elastic stiffness tensor C_{ij} (GPa), the density ρ ($10^3\ kg/m^3$) and the thickness e (mm) for the CFRP layer are cited from [12] and listed in Table 1.

For the Aluminum layer we have: $E = 72.4\ GPa$; $e = 1\ mm$; $\rho = 2770\ kg/m^3$; $\nu = 0.33$.

a) The balancing algorithm's effectiveness and validation

To evaluate the effectiveness of our algorithm, we will use two indicators: the matrix norm and the conditioning measure. These were generated before and after the application of balancing. The Norm function represents the first indicator, while the Cond

function represents the second.

Tables 2 and 3 present the balancing effect on the matrix system of the eigenvalue problem. For a wavenumber of $k = 1\ rad/mm$ and two different values of collocation points N, Table 2 shows a decrease in balance signs, indicating good balancing. The same reduction norm is observed in the M matrix.

The effectiveness of the balancing approach in straightening and correcting eigenvalues by reducing relative error (RE) was examined. Table 3 demonstrates that inaccurate frequency values of ω_1 hinder the creation of precise curves. Balancing reduce RE, allowing values of ω_2 to closely approximate the DC values of ω_{DC}.

b) Dispersion curves of [CFRP-Al- CFRP-Al]

The dispersion curves in Fig. 7 illustrate the balancing improvement through good agreement with the DC results. In Fig. 7(a), the cutoff frequency zone highlights the missing solutions in DC plot caused by the curves' conversion from phase velocity (V_p) space to wavenumber (k) space.

In this section, we can conclude that the balancing algorithm is an efficient preconditioner for our eigenvalue problem. The following results evaluate our algorithm.

4.1.2. Dispersion curves of Hybrid multi-layer composites [CFRP-Al]₅₀

The second example for verification involves a hybrid system with a high number of layers. The layup [CFRP-Al]₅₀ combines orthotropic material with the properties listed in Table 4 and isotropic material. The results in Fig. 8 demonstrate good agreement between the SCM and DC.
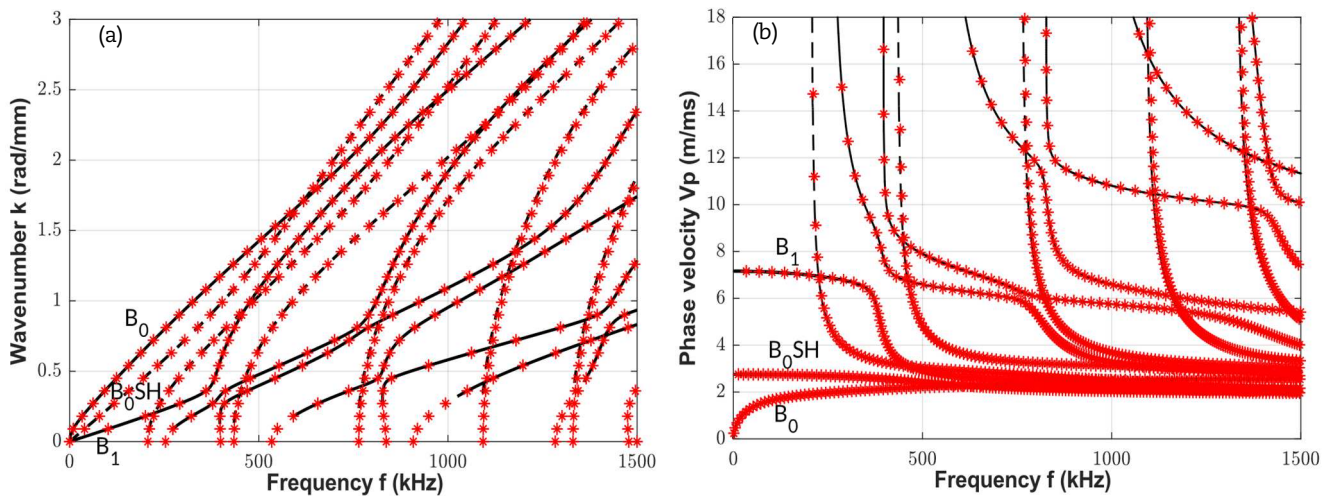
Fig. 7. Coupled modes dispersion curve (Lamb and SH) in [CFRP-Al-CFRP-Al] in the (k,f) plane (a) and the (V_p,f) plane (b). Plotted by: SCM (stars) with N=20, DC software (solid lines).
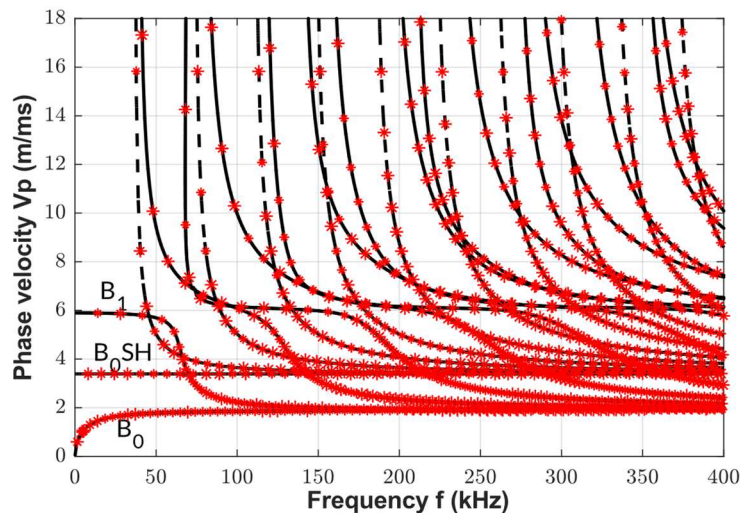

Fig. 8. Coupled modes dispersion curve in the hybrid layered composite [CFRP-Al]₅₀, plotted by: SCM (stars) with N = 4, DC software (solid lines in blue).

Table 4. Proprieties of the orthotropic CFRP layer.

C_{11}	C_{22}	C_{33}	C_{12}	C_{13}	C_{23}	C_{44}	C_{55}	C_{66}	e	ρ
70	33	14.7	23.9	6.2	6.8	4.2	4.7	21.9	1	1.5

Table 5. Proprieties of the transversely isotropic plate T800M913.

C_{11}	C_{22}	C_{33}	C_{12}	C_{13}	C_{23}	C_{44}	C_{55}	C_{66}	e	ρ
154	9.5	9.5	3.7	3.7	5.2	2.15	4.2	4.2	1	1.55

4.2. Transversely isotropic Multi-layered composites T800M913 [0/90]$_x$

4.2.1. Multi-layered composite T800M913 [0/90/0/90]

a) Number of collocation points and thickness effect on convergence rate

The material chosen for this study is T800M913, a unidirectional layer of the fiber-matrix system commonly used in the field of solid mechanics and NDT. This material has been previously studied by experts [33, 34] and is included in the material library of DC software. It belongs to the class of materials with hexagonal symmetry and its material properties are determined by five elastic constants. For this case, the T800M913 was rotated to correspond with the layup [0/90/0/90]. The technical properties corresponding to this layup are listed in Table 5.

The decimal logarithm of the relative error RE in terms of the frequency ω is computed for the 4 mm thick layered composite [0/90/0/90], the DC solutions are taken as reference, see Fig. 9, and has the relation: $\text{Re} = |\omega - \omega_{DC}| / \omega_{DC} \times 100$. The results demonstrate a significant reduction in error as N increases in both fundamental mode B_0 and high order mode B_9.

After evaluating the effect of spectral discretization on plot precision, we investigated the relationship between the running time for plotting dispersion curves and the thickness in the asymmetric multilayer composite T80M913[0/90]$_x$. The total thickness is increased by adding layers (i.e., increasing x) with a thickness of 0.25 mm. The study is conducted for three values of collocation points N, as shown in Fig. 10, within a thickness range of 10 mm. The computer used for this study has an Intel Ci7-6820HQ processor running at 2.7 GHz and 8 GB of RAM. In SCM, the number of discretization points N per layer remains constant for all layers. We chose a wavenumber step of 100 m^{-1} and a final value of 6000 m^{-1}.

It was anticipated that an increase in the total thickness H would result in a greater number of collocation points, leading to longer computation times. This sluggishness is due to the increase in matrix size and the quantity of boundary conditions that need to be verified.

b) Dispersion curves of T800M913 [0/90/0/90]

Figure 11 shows a wavenumber plot that is accurate and consistent with the DC plot. The dispersion curves appear to cross each other, but upon closer examination (as seen in the inset image), it is clear that two modes are passing very close to each other without actually crossing. Figure 12 displays the phase velocity plot, which also demonstrates good accuracy.
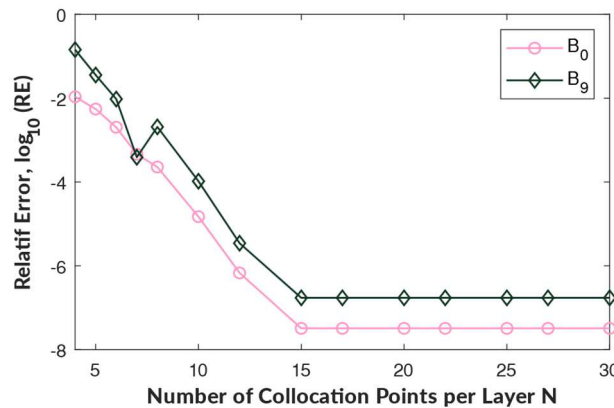

Fig. 9. Decimal logarithm of the RE in computed frequency at $k = 1$ rad/mm as a function of the number of collocation points per layer for the B_0 and B_9 modes.
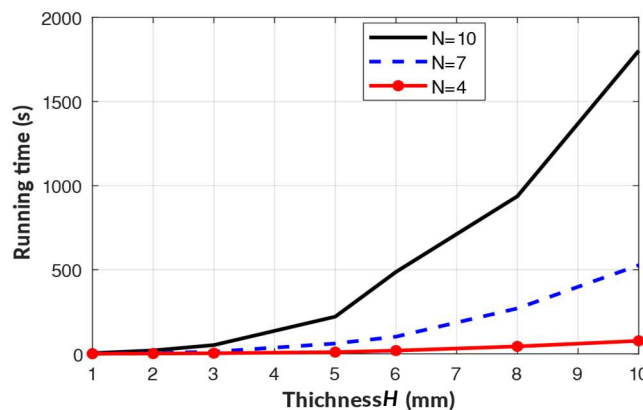

Fig. 10. Running time evolution with thickness for the layered composite of T800M913[0/90]$_x$. Three values of collocation points N are considered.
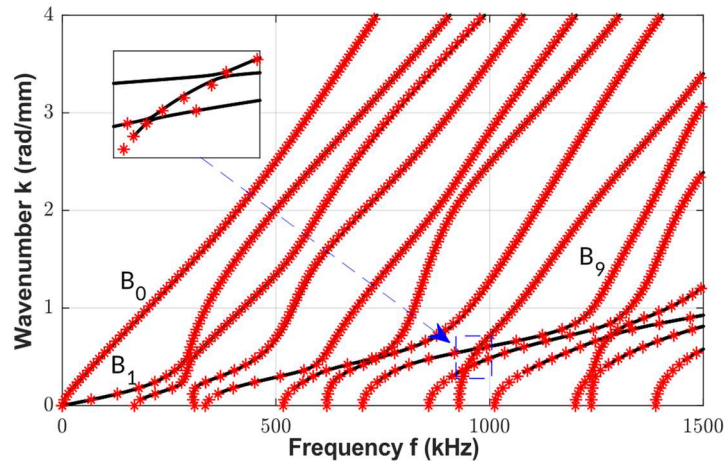
Fig. 11. Lamb modes dispersion curve in the T800M913 [0/90/0/90], plotted by: SCM (stars) with $N = 10$, DC software (solid lines). The inset is a magnification of the small discontinued rectangular.
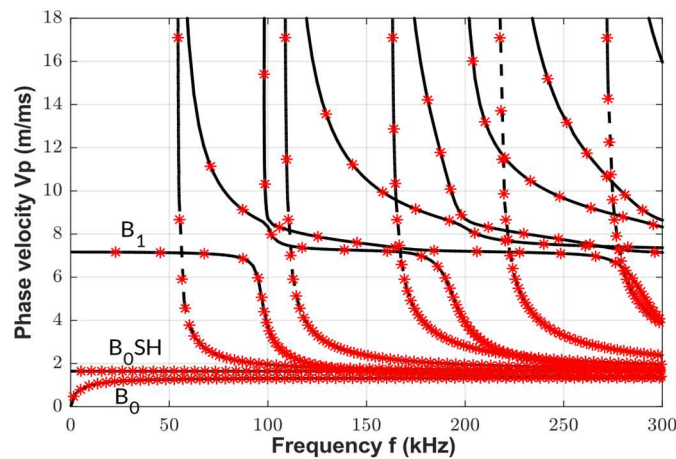

Fig. 12. Coupled modes dispersion curve in the T800M913[0/90]25, plotted by: SCM (stars) with $N = 4$, DC software (solid lines).
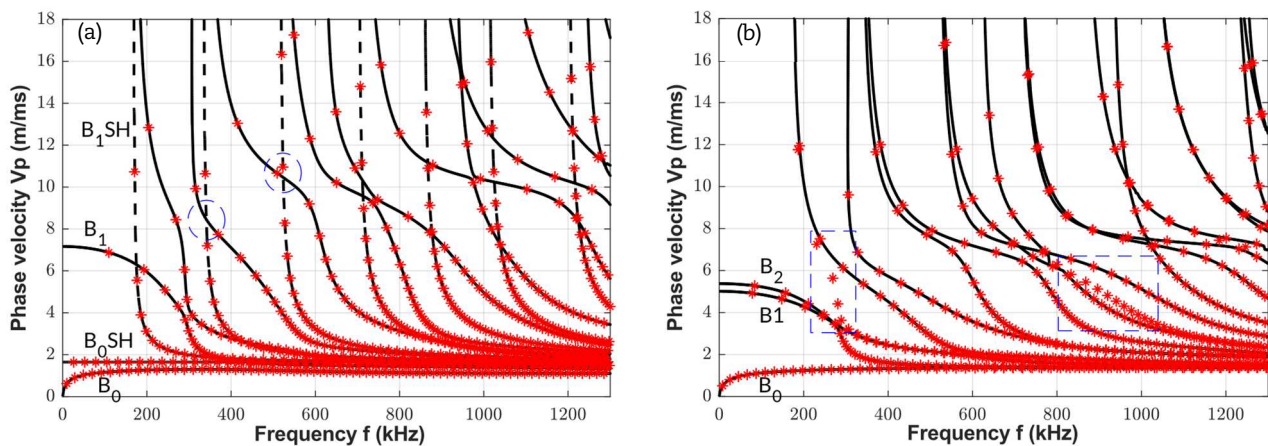

Fig. 13. Coupled modes dispersion curve in 4 mm thick of T800M913 [0/90/0/90], plotted by: SCM (stars) with $N = 10$, DC software (solid lines). (a) $\theta = 0$ degree, (b) $\theta = 45$ degrees.

c) Guided wave directional dependency

It is widely recognized in the NDT that the dispersion characteristics of different modes are closely related to the wave propagation direction θ. Figure 13 analyzes the phase velocity results for waves propagating in two separate directions at 0 degree and 90 degrees with respect to the global direction x_1. The results of the SCM and SMM were identical.

Figure 13(b) shows that due to the asymmetric layup, mode separation cannot be achieved. Therefore, we use the letter 'B' to denote the coupled modes of Lamb and SH. The rectangular zones indicate that DC misses modes B_3 and B_8, and a finer frequency step is required to identify parts of them. However, such manual interventions are unnecessary for SCM. Figure 13(a) shows the intersection of several higher order modes (branches with cut-off frequencies) at approximately 340 kHz and 520 kHz, as indicated by the circles. However, these branches separate in this area as the angle of propagation increases to 0 degree.
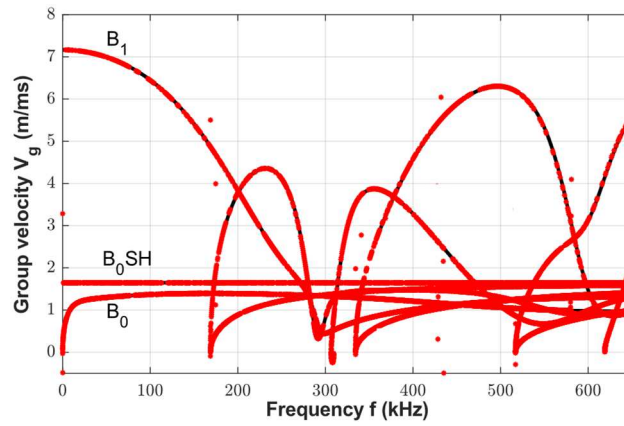
Fig. 14. Coupled modes dispersion curve in 4 mm thick of T800M913 [0/90/0/90], plotted by: SCM (stars) with $N = 10$, DC (solid lines). Along $\theta = 0$ deg.
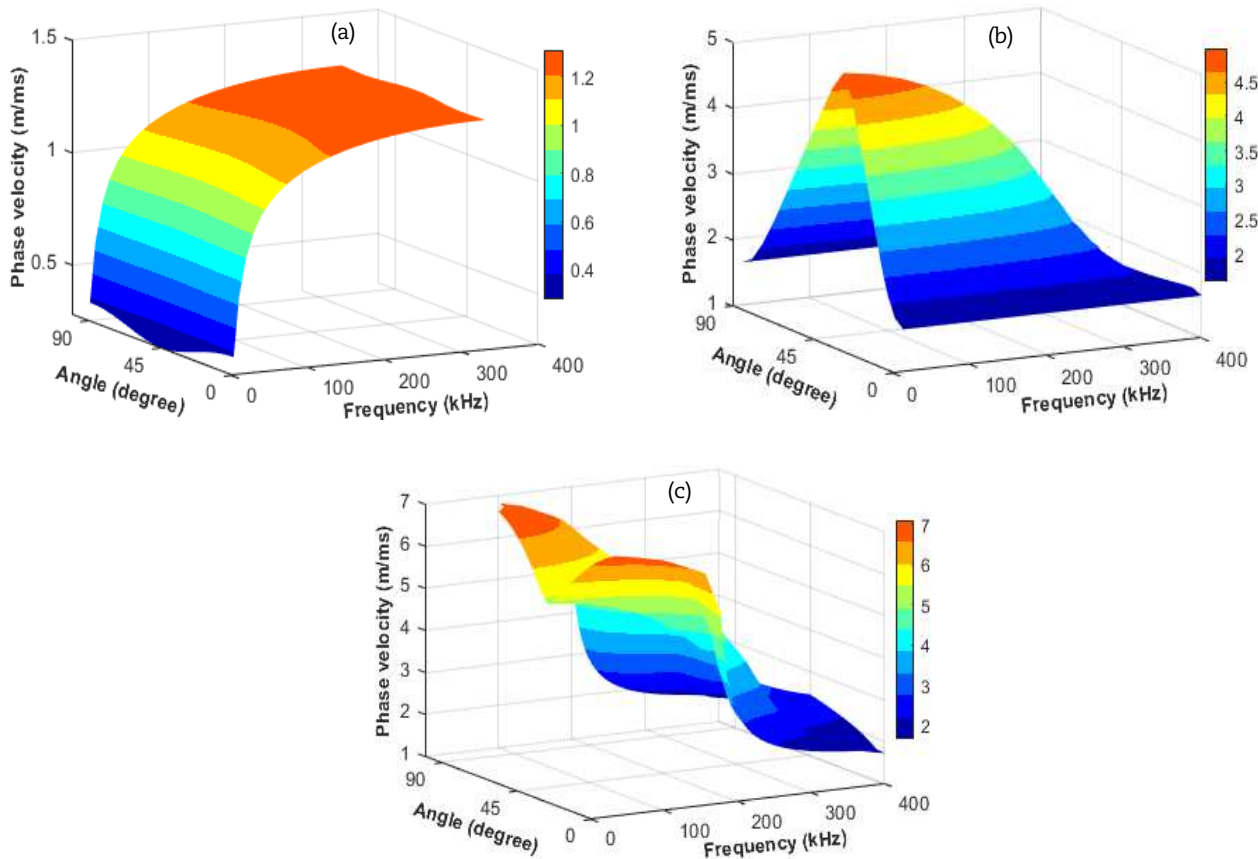

Fig. 15. Phase velocity as a function of frequency and propagation angle in the T800M913[0/90/0/90]. (a) B_0 mode, (b) B_1 mode, (c) B_2 mode, plotted by: SCM with $N = 10$. For a color version, see the plates section.

The B_0^{SH} mode exhibits non-dispersive behavior with a constant phase velocity of $V_p = \sqrt{c_{66}/\rho} = 1.65 \ m/ms$ when propagating along the 0 degree direction. However, when the propagation direction is changed, the same mode transforms into a coupled B_1 mode with some degree of dispersion, as seen in Fig. 13(b). At 90 degrees it resumes its horizontal transverse speed, as shown in Fig. 14(b). Furthermore, according to Fig. 14(c), mode B_2 experiences a speed reduction at a 45-degree angle, possibly due to the weakening of stiffness constants in this direction of propagation compared to the direction of the fibers, as shown in Fig. 3.

The group velocity can be computed using the relationship, $V_g = \frac{d\omega}{dk}$, and the dispersion curve is presented in Fig. 14 showing good concordance with SMM.

d) Displacement and stress profiles of T800M913 [0/90/0/90]

Two points were selected from the dispersion curve of the T800M913[0/90/0/90] composite, corresponding to the coupled fundamental modes B_0 and B_1 at a frequency of 500 kHz. These positions are designated by the circles in Fig. 16. The eigenvectors in Eq. (22) represent the displacement profiles created by the SCM at these positions. The eigenvector balancing phase, as shown in Eq. (21), was crucial to obtaining the desired results. Figures 17 and 18 show a close result with DC, where the stress field and displacement profiles are continuous across the thickness. Although the form of the displacement profiles has been successfully recovered, the balancing procedure has caused a decline in the accuracy of the eigenvectors. This issue is discussed in [35].

To plot displacement profiles of the spectral method, normalization by the acoustic power is applied, as described in [28, 34]. This processing step provides a precise and objective interpretation of the results.
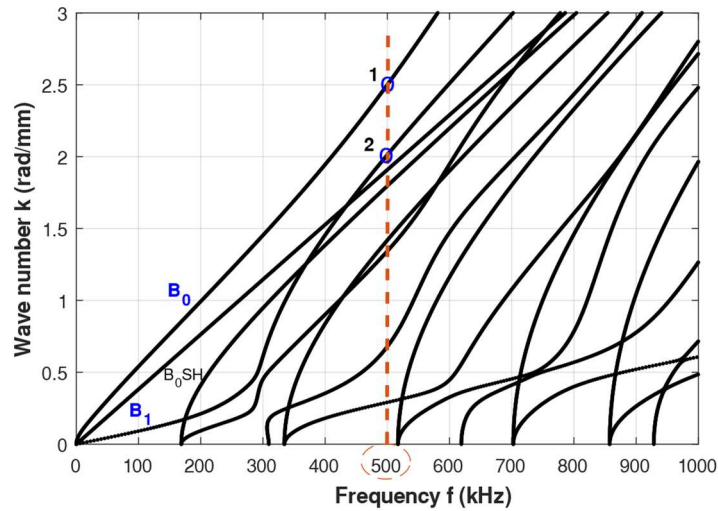
Fig. 16. Coupled modes in 4 mm of T800M913 [0/90/0/90], plotted by SCM, $N = 30$. Indication with circles of two mode shapes points at 500 kHz frequency.
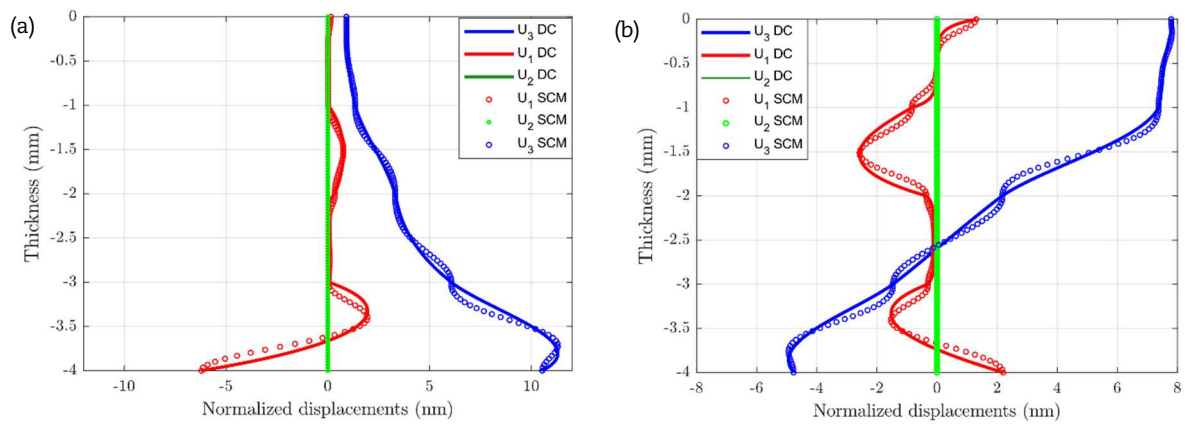

Fig. 17. Wave structures of the B_0 (a) and B_1 (b) modes localized at the frequency $f = 500$ kHz and $N = 30$.
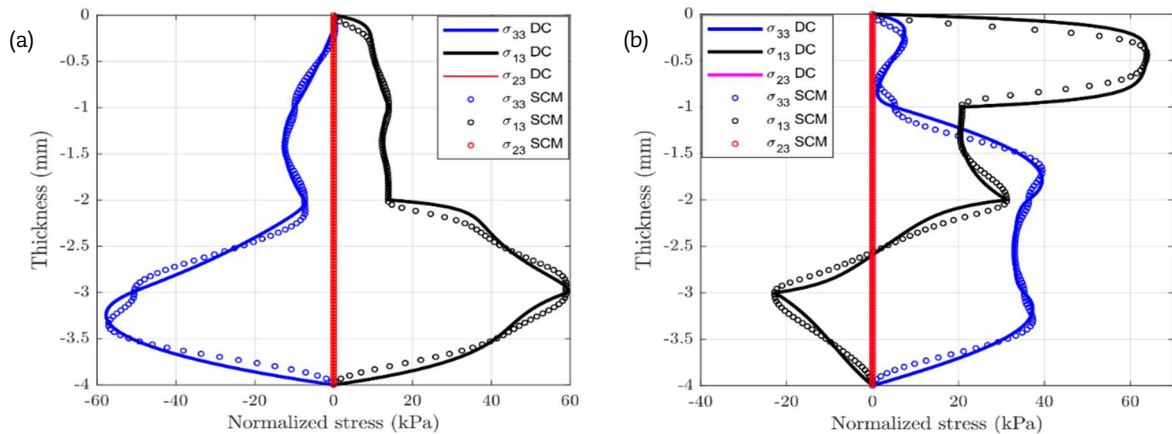

Fig. 18. Stress profiles of the B_0 (a) and B_1 (b) modes localized at the frequency $f = 500$ kHz and $N = 30$.

Figure 17 shows that component u_2 of B_0 and B_1 modes vanish, transforming them into pure Lamb waves. Furthermore, these modes are dominated by normal displacement u_3. Consequently, at the concerned frequency range, the phase velocity of these modes approaches that of the pure longitudinal bulk wave (B_0^{SH}), as shown in Fig. 13(a). Additionally, Fig. 18 displays the stress field produced by B_0 and B_1 modes at the same frequency. The free composite boundary conditions are verified for the out-of-plane component σ_{33} and the shear components σ_{13} and σ_{23}. When compared to the DC result, the SCM produces a satisfactory result.

4.2.2. Dispersion curves of transversely isotropic multi-layered composite T800M913 [0/90]$_{10s}$

The efficiency of the SCM with balancing strategy is evaluated in this study by applying it to a symmetric multi-layered composite. To ensure accurate results, boundary conditions (BC) were carefully inserted into the global matrix $\mathcal{L}$ and the matrices in Eq. (13) were assembled with the BCs reversed from the composite's line of symmetry. The composite's symmetry enables mode separation. The shear horizontal modes (SH) are separated from the Lamb modes by evaluating the second component of the calculated eigenvectors along x_2. The symmetrical and asymmetrical modes are distinguished by evaluating the signs of the other eigenvector components. This mode separation for the T80M913 [0/90]$_{10s}$ composite is illustrated in Fig. 19 and Fig. 20.
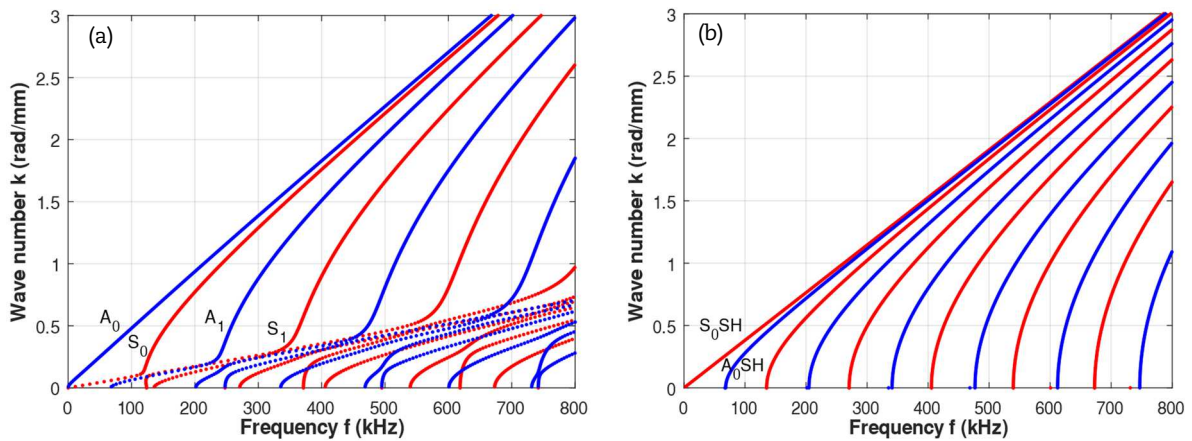
Fig. 19. Decoupled modes dispersion curve by SCM in the symmetric layered composite T80M913[0/90]$_{10s}$. (a) Lamb modes, (b) SH modes. Symmetric modes (in red) and asymmetric modes (in blue).
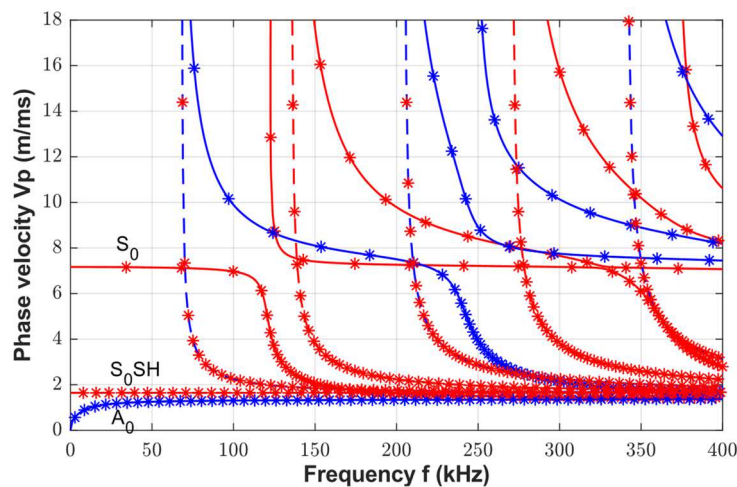

Fig. 20. Decoupled modes dispersion curve in the layered composite T80M913[0/90]$_{10s}$, plotted by: SCM (stars) with N = 4, DC software (solid lines in blue). Symmetric modes (in red) and asymmetric modes (in blue).
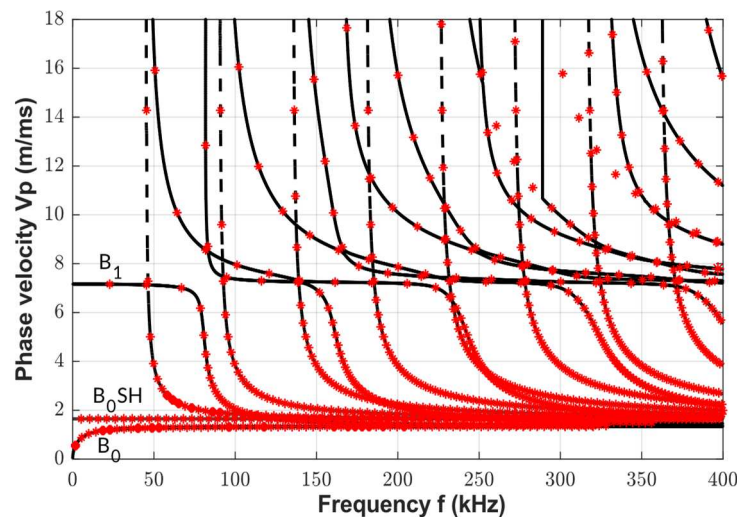

Fig. 21. Coupled modes dispersion curve in the layered composite T800M913[0/90]$_{100}$, plotted by: SCM (stars) with N = 4, DC software (solid lines).

4.2.3. Dispersion curves of transversely isotropic multi-layered composite T800M913 [0/90]$_{100}$

As in a previous study on DC software [34, 36], we are conducting a challenging layup with 200 layers and a thickness of 25 mm. This composite material is commonly used in the aircraft industry. Additionally, the coupling of Lamb and SH modes presents a challenge for the plotting algorithms due to mode crossings. The purpose of the SCM is to calculate the dispersion curve of phase velocity in terms of wave number k. The steps are set at 15 m/s up to a maximum of 1800 m/s with N = 4 per layer. The plot demonstrates excellent agreement with DC's results, as shown in Fig. 21, except for the 250-350 kHz frequency range, where the DC fails to plot a branch of modes. This requires additional computing time due to the need for a finer step in DC. It has been concluded that the SCM can handle a greater number of layers and various configurations.

5. Conclusion

The study conducted here aimed to optimize the spectral collocation method for composite waveguides in ultrasonic non-destructive testing. The paper demonstrates that using a balancing algorithm to solve the eigenvalue problem of the SCM is an effective tool for calculating dispersion curves and displacement/stress profiles. Previous works on the SCM, such as [20, 29], have not addressed the numerical instabilities that we have highlighted. These instabilities are caused by the method used to construct the matrix system that defines the eigenvalue problem. The proposed algorithm for balancing has significantly reduced both the conditioning measure and the matrix norm in the matrix system, optimizing the spectral formulation and enabling accurate solutions to be calculated. This ensures reliability and ease of implementation of the SCM in complex composite structures.

The accuracy of the balanced-SCM was demonstrated at both low and high frequencies by selecting the fundamental mode B_0 and the higher order mode B_9 to assess the plotting error. An error of less than 0.03% was achieved with only 20 collocation points per layer. Subsequently, various multilayer configurations were examined, and the plotting results were consistent with those of DC. However, when dealing with a large number of layers, we observed a decrease in the computational cost of the SCM. This is explained by the discretization of the domain, which increases matrix sizes, as well as the multiplication of boundary conditions and interfaces that need to be verified. Nevertheless, the method's robustness is always preserved, as it can calculate all propagating modes with a separation into Lamb and SH, symmetric and anti-symmetric modes. In addition, SCM has been shown to overcome the limitations of traditional zero-finding methods by computing dispersion curves for laminates with 200 layers with high precision and good convergence. Furthermore, the balanced SCM successfully extracted displacement profiles and stress fields, allowing for effective use of ultrasonic non-destructive testing on multi-layered composites which are of great interest in the aeronautical and space industries. The study's findings support previous research and validate SCM's competitiveness when compared to other methods such as SMM, GMM, and SAFE.

There is room for further work. Only planar structures were examined in this study due to their prominence and relevance in the industry. However, it is important to note that cylindrical structures should also be taken into account since the principle of assembling the matrices remains the same. Furthermore, a comparison can be made with other balancing algorithms, such as those discussed in [39], in terms of processing time and accuracy of the calculated eigenvalues. The method presented here can be used to analyze dispersion curves and wave structures in a multilayered composite with an imperfect interface, such as delamination.

Author Contributions

The project scheme was planned by M. Mekkaoui and H. Rhimini. M. Mekkaoui performed the design, implementation, programming, and analysis of the research. Theory validation was examined by M. Mekkaoui and S. Nissabouri. All authors discussed the results, reviewed, and approved the final version of the manuscript.

Acknowledgments

Conflict of Interest

The authors declared no potential conflicts of interest concerning the research, authorship, and publication of this article.

Funding

Data Availability Statements

Not Applicable.

Nomenclature

h	Thickness of a single layer [m]	V_p	Phase velocity [m/s]
L_c	Length of n-layers system [m]	V_g	Group velocity [m/s]
H	Total thickness of n-layers system [m]	U_i	Displacement components (i = 1, 2, 3) [m]
$\varnothing$	Fiber direction of a single layer [Degree]	σ_{ij}	Stress components (i,j = 1, 2, 3) [Pa]
θ	Direction of wave propagation [Degree]	ρ	Density [kg/m^3]
ω	Angular frequency [rad/s]	E	Young's modulus [Pa]
f	Frequency [Hz]	ν	Poisson ratio
k	Wavenumber [1/m]	C_{ij}	Stiffness components [Pa]

References

[1] Rose, J.L., Ed., *Ultrasonic Guided Waves in Solid Media*, Cambridge University Press, 2014.
[2] Lamb, H., On waves in an elastic plate, *Proceedings of the Royal Society of London. Series A, Containing papers of a mathematical and physical character*, 93(648), 1997, 114–128.
[3] Thomson, W.T., Transmission of Elastic Waves through a Stratified Solid Medium, *Journal of Applied Physics*, 21(2), 2004, 89–93.
[4] Haskell, N.A., The dispersion of surface waves on multilayered media, *Bulletin of the Seismological Society of America*, 43(1), 1953, 17–34.
[5] Nayfeh, A.H., The general problem of elastic wave propagation in multilayered anisotropic media, *The Journal of the Acoustical Society of America*, 89(4), 1991, 1521–1531.
[6] Knopoff, L., A matrix method for elastic wave problems, *Bulletin of the Seismological Society of America*, 54(1),1964, 431–438.
[7] Rokhlin, S.I., Wang, L., Stable recursive algorithm for elastic wave propagation in layered anisotropic media: Stiffness matrix method, *The Journal of*

the Acoustical Society of America, 112(3), ,2002, 822–834.

[8] Lowe, M.J.S., Matrix techniques for modeling ultrasonic waves in multilayered media, *IEEE Transactions on Ultrasonics, Ferroelectrics, and Frequency Control*, 42(4), 1995, 525–542.

[9] Barski, M., Pajak, P., Determination of Dispersion Curves for Composite Materials with the Use of Stiffness Matrix Method, *Acta Mechanica et Automatica*, 11(2), 2017, 121–128.

[10] Guo, S., Rébillat, M., Liu, Y., Li, Q., Lu, C., Mechbal, N., Guided waves propagation in arbitrarily stacked composite laminates: Between-layers incompatibility issue resolution using hybrid matrix strategy, *Composite Structures*, 322, 2023, 117360.

[11] Sorokin, S.V., Broberg, P.H., Steffensen, M.T., Ledet, L.S., Finite element modal analysis of wave propagation in homogeneous and periodic waveguides, *International Journal of Mechanical Sciences*, 227, 2022, 107444.

[12] Rhimini, H., Bougaze, B., El Ouahdani, M., Sidki, M., Nassim, A., Modelling of Lamb waves propagation in plane plates by the finite element method, *Physical and Chemical News*, 46, 2009, 63–72.

[13] Nissabouri, S., El Allami, M., Boutyour, E., Ahmed, E., Lamb wave interaction with delamination in orthotropic plate, *ACM International Conference Proceeding Series, Larache*, Morocco, 1–5, 2017.

[14] Mace, B., Manconi, E., Modelling wave propagation in two-dimensional structures using finite element analysis, *Journal of Sound and Vibration*, 318, 2008, 884–902.

[15] Bartoli, I., Marzani, A., Lanza di Scalea, F., Viola, E., Modeling wave propagation in damped waveguides of arbitrary cross-section, *Journal of Sound and Vibration*, 295, 2006, 685–707.

[16] Giurgiutiu, V., Haider, M.F., Propagating, Evanescent, and Complex Wavenumber Guided Waves in High-Performance Composites, *Materials*, 12(2), 2019, 269.

[17] Nissabouri, S., El Allami, M., Boutyour, E., Quantitative evaluation of semi-analytical finite element method for modeling Lamb waves in orthotropic plates, *Comptes Rendus Mécanique*, 348(5), 2020, 335–350.

[18] Dahmen, S., Amor, M.B., Ghozlen, M.H.B., Investigation of the coupled Lamb waves propagation in viscoelastic and anisotropic multilayer composites by Legendre polynomial method, *Composite Structures*, 153, 2016, 557–568.

[19] Adamou, AT.I., Craster, R. V., Spectral methods for modelling guided waves in elastic media, *The Journal of the Acoustical Society of America*, 116(3), 2004, 1524–1535.

[20] Karpfinger, F., Valero, H., Gurevich, B., Bakulin, A., Sinha, B., Spectral-method algorithm for modeling dispersion of acoustic modes in elastic cylindrical structures, *Geophysics*, 75(3), 2010, H19–H27.

[21] Karpfinger, F., Gurevich, B., Bakulin, A., Modeling of wave dispersion along cylindrical structures using the spectral method, *The Journal of the Acoustical Society of America*, 124(2), 2008, 859–865.

[22] Hernando Quintanilla, F., Lowe, M.J.S., Craster, R.V., The symmetry and coupling properties of solutions in general anisotropic multilayer waveguides, *The Journal of the Acoustical Society of America*, 141(1), 2017, 406-418.

[23] Georgiades, E., Lowe, MJ. S., Craster, R.V., Identification of leaky Lamb waves for waveguides sandwiched between elastic half-spaces using the Spectral Collocation Method, *The Journal of the Acoustical Society of America*, 155, 2023, 629-639.

[24] Ward, R.C., Balancing the Generalized Eigenvalue Problem, *SIAM Journal on Scientific and Statistical Computing*, 2(2), 1981, 141–152.

[25] Dispersion Calculator Armin Huber DLR-homepage, 2020.

[26] Weideman, JA., Reddy, S.C., A MATLAB differentiation matrix suite, *ACM Transactions on Mathematical Software*, 26(4), 2000, 465–519.

[27] Zitouni, I., Rhimini, H., Chouaf, A., Modeling the Propagation of Ultrasonic Guided Waves in a Composite Plate by a Spectral Approximation Method, *Engineering Transactions*, 71(2), 2023, 213-227.

[28] Zitouni, I., Rhimini, H., Chouaf, A., Comparative Study of the Spectral Method, DISPERSE and Other Classical Methods for Plotting the Dispersion Curves in Anisotropic Plates, *Journal of Applied and Computational Mechanics*, 9(4), 2023, 955–973.

[29] Quintanilla, F.H., Fan, Z., Lowe, M.J.S., Craster, R.V., Guided waves' dispersion curves in anisotropic viscoelastic single- and multi-layered media, *Proceedings of the Royal Society A: Mathematical, Physical and Engineering Sciences*, 471(2183), 2015, 20150268.

[30] Householder, A.S., *The Theory of Matrices in Numerical Analysis*, Blaisdell, New York, 1964, Reprinted by Dover, New York, 1975.

[31] Nayfeh, A.H. Chimenti, D.E., Free Wave Propagation in Plates of General Anisotropic Media, *Journal of Applied Mechanics*, 56(4), 1989, 881–886.

[32] Pavlakovic, B., Lowe, M., Alleyne, D., Cawley, P., Disperse: A General Purpose Program for Creating Dispersion Curves, *Review of Progress in Quantitative Nondestructive Evaluation*, 16A, 1997, 185–192.

[33] Rautela, M., Huber, A., Senthilnath, J., Gopalakrishnan, S., Inverse characterization of composites using guided waves and convolutional neural networks with dual-branch feature fusion, *Mechanics of Advanced Materials and Structures*, 29(27), 2022, 6595–6611.

[34] Huber, A., *Numerical Modeling of Guided Waves in Anisotropic Composites with application to Air-coupled Ultrasonic Inspection*, Ph. D. Thesis, Faculty of Mathematics, Natural Sciences and Technology, University of Augsburg, 2023.

[35] James, R., Langou, J., Lowery, B.R., On matrix balancing and eigenvector computation, *arXiv*, 2014.

[36] Huber, A., Classification of solutions for guided waves in fluid-loaded viscoelastic composites with large numbers of layers, *The Journal of the Acoustical Society of America*, 154(2), 2023, 1073–1094.

[37] Auld, B.A., *Acoustic fields and waves in solids*, Krieger Publishing Company, Malabar, FL, 1990.

[38] Kamal, A., Giurgiutiu, V., Stiffness Transfer Matrix Method (STMM) for stable dispersion curves solution in anisotropic composites, *Health Monitoring of Structural and Biological Systems*, 9064, 2014, 293-306.

[39] Longsine, D.E., McCormick, S.F., Simultaneous Rayleigh quotient minimization methods for Ax=λBx, *Linear Algebra and its Applications*, 34, 1980, 195-234.

ORCID iD

Moussa Mekkaoui https://orcid.org/0009-0001-5775-970X
Salah Nissabouri https://orcid.org/0000-0001-7702-3030
Hassan Rhimini https://orcid.org/0000-0002-5784-9844

Publisher's Note Shahid Chamran University of Ahvaz remains neutral with regard to jurisdictional claims in published maps and institutional affiliations.